THE JOURNAL OF PHYSICAL CHEMISTRY B
A JOURNAL OF THE AMERICAN CHEMICAL SOCIETY

pubs.acs.org/JPCB

Article

Electrical Conductivity Differences between Experiments and Classical Simulations Reveal Self-Diffusion Coefficients and Ion Lifetimes of Hydroxide and Hydronium in Aqueous Solutions

V. Jelle Lagerweij, Othonas A. Moultos, and Thijs J.H. Vlugt*

Cite This: *J. Phys. Chem. B* 2026, 130, 1332–1345

Read Online

ACCESS | Metrics & More | Article Recommendations | Supporting Information

ABSTRACT: Grotthuss transfer is responsible for a large increase in the self-diffusion of hydroxide and hydronium ions in aqueous solutions compared to similarly sized ions. Recent advances in machine-learning molecular dynamics have shown some success in capturing this process. In the present work, we show that classical molecular dynamics combined with experimentally measured electrical conductivities can also be used to determine self-diffusion coefficients and the lifetimes of hydroxide and hydronium ions in aqueous KOH, NaOH, and HCl solutions. This was tested and validated across a wide range of concentrations at 25 and 60 °C. The approach relies on augmenting classically computed trajectories with a biased random walk, which together accounts for both vehicular transport and Grotthuss transfer. The concentration and temperature dependence of this random walk are calibrated by comparing simulated electrical conductivities with available experimental electrical conductivity data. The computed self-diffusion coefficients match measurements at infinite dilution and results from machine learning molecular dynamics. Ion lifetimes reported by machine learning and ab initio molecular dynamics studies depend strongly on the precise definition of what constitutes a Grotthuss transfer event. Our approach for calculating ion lifetimes does not have this drawback. We also show that our self-diffusion coefficients and electrical conductivities are insensitive to the precise definition of what constitutes a Grotthuss transfer event.

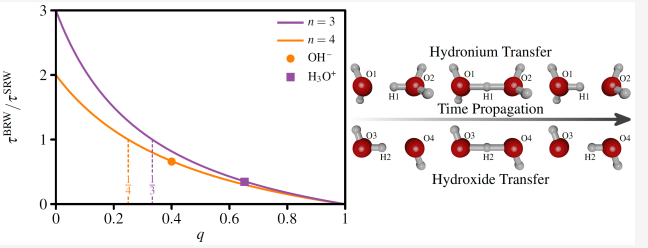

1. INTRODUCTION

Aqueous salt solutions have always been of great industrial relevance.[1] Salt mixtures containing hydroxide or hydronium ions in aqueous solutions, such as potassium hydroxide, sodium hydroxide, and hydrochloric acid are of particular interest due to proton hopping (also referred to as Grotthuss transfer).[2−5] This is a unique transport mechanism first described by Grotthuss in 1806 that significantly enhances ion diffusion and therefore electrical conductivity, compared to similarly sized ions that do not have Grotthuss transfer.[2−5] Grotthuss transfer involves a molecular identity switch, where a proton is exchanged between the transferring ion and a water molecule,[2,3,6] as illustrated in Figure 1. This proton exchange between neighboring molecules effectively moves charge without requiring molecular diffusion. This charge-hopping process significantly enhances overall charge transport. As a result, electrolytes exhibiting strong Grotthuss-type conduction are particularly valuable in systems where minimizing conductive losses is critical, such as in alkaline and acidic electrolysis,[7,8] batteries,[9] and CO_2 reduction.[10] Accurately determining the extent to which Grotthuss transfer contributes to conductivity and ion self-diffusion coefficients offers a fundamental understanding of electrolyte behavior, which can guide development of more efficient industrial processes.

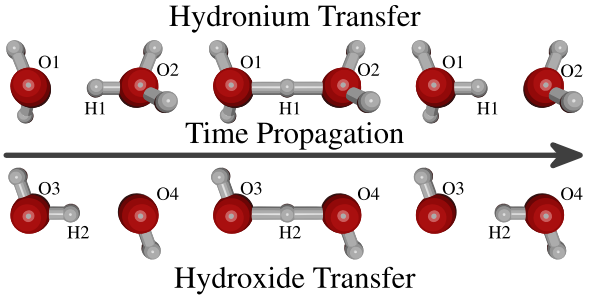

Figure 1. Grotthuss transfer of hydronium and hydroxide in aqueous solutions. (Top) Before the reaction (i.e., proton transfer) occurs, the central atom of the hydronium is O2. During the reaction, H1 transfers to O1, which is then the central atom of the hydronium. (Bottom) The oxygen in the hydroxide is O4, the proton transfer of H2 toward O4 changes the hydroxide into a water molecule, so that then O3 is the central atom of the hydroxide. The atomic positions change only slightly in both transfer events. This results in significant charge transfer in a short time frame as the ion effectively swaps identity with a water molecule.

Received: October 17, 2025
Revised: December 17, 2025
Accepted: January 5, 2026
Published: January 20, 2026

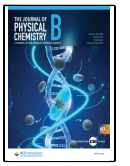

https://doi.org/10.1021/acs.jpcb.5c07132
J. Phys. Chem. B 2026, 130, 1332–1345

Investigating the self-diffusion coefficients of Grotthuss transferring ions experimentally is challenging. The proton exchange changes the atoms that make up the specific ions, as shown in Figure 1. This makes it impossible to measure self-diffusion coefficients using isotope traces as often used for other ions.[11] While measuring the self-diffusion coefficients of OH^- and H_3O^+ directly has been challenging, this has not been the case for electrical conductivity, which can be measured directly following a relatively simple process, as it is a macroscopic property.[12] Therefore, electrical conductivities of NaOH(aq) KOH(aq), and HCl(aq) are available for multiple temperatures and concentrations.[13,14] Assuming no ion−ion correlations, the approximate relation between electrical conductivity and ion self-diffusion coefficients has long been known.[15,16] This assumption only applies at infinite dilution, as at higher electrolyte concentrations, cross-correlations between all ions contribute to the electrical conductivity.[16,17] Therefore, self-diffusion coefficients of OH^- and H_3O^+ are only estimated from the ionic conductivities at infinite dilution.[15,18]

Studying Grotthuss transfer via molecular simulation is also challenging, where computational expenses and accuracies in interatomic interactions are the most pressing issues. Most simulations of Grotthuss transfer were performed using ab initio molecular dynamics (AIMD).[3,4,19−21] Most of the AIMD studies investigated the hydrogen bonding network before and during the Grotthuss transfer events,[3,4,6,19] and for example revealed that a specific hydrogen bonding network around the OH^- or H_3O^+ is required for the transfer to take place.[6] The high computational cost of AIMD restricts its use to short time- and length scales. Classical force field-based MD is computationally more efficient, enabling simulations for larger systems and longer time scales. Classical force fields do not consider chemical reactions and thus cannot describe the Grotthuss transfer of OH^- and H_3O^+ accurately. The approach of combining Monte Carlo trial moves in which Grotthuss transfer events are attempted into classical MD simulations has shown some success in modeling Grotthuss transfer.[22−26] However, this requires fitting energy barriers to the ion self-diffusion coefficients, which are only available at infinite dilution or require long, computationally expensive AIMD simulations. Recent advances into Machine-Learned Interatomic Potentials (MLIP) have resulted in renewed interest in Grotthuss transfer.[6,27,28] MLIPs provide near ab initio quality with a significant reduction in computational expenses compared to AIMD, making larger simulation time and length scales accessible through Machine Learning Molecular Dynamics (MLMD).[29] Computations of electrical conductivities of KOH(aq), research on concentration effects of NaOH(aq) on Grotthuss transfer, and detailed studies of H_3O^+ energy barriers have all been published within the past decade.[6,27,28,30] Despite achieving significant success in modeling Grotthuss transfer, MLIPs still present several disadvantages: (1) While computationally more efficient than ab initio techniques, MLIPs require more computational resources than classical force fields. For example, simulating a system of 1000 water molecules for 100 ns with the most up-to-date version of DeePMD-kit (V3) takes more than 80 days on a single NVIDIA H100 GPU.[31] Therefore, it is not yet practical to screen transport properties (i.e., self-diffusion coefficients and electrical conductivities) of multicomponent mixtures at multiple concentrations and temperatures. (2) The aforementioned studies[22,23,25,26] used MLIPs without long-ranged electrostatics. It has been shown that MLIPs with explicit long-range electrostatics provide higher accuracies in simulations of aqueous systems.[32,33] (3) The quality of MLIPs depends on the accuracy of the ab initio training data. Errors in ab initio methods carry over into MLIPs. AIMD and MLMD simulations usually overestimate the density of liquid water, even for highly accurate metaGGA and hybrid methods such as SCAN and SCAN0.[34] Many studies using MLMD methods only simulate in the *NVT* ensemble using experimental densities,[6,28] instead of using *NPT* to retrieve the density and then continue with *NVT* or *NVE* to sample observables.

While classical force fields cannot capture Grotthuss transfer itself, this limitation can be turned into a strength. Classical MD simulations of aqueous ion solutions accurately describe the vehicular transport (i.e., Brownian diffusion of unreacting molecular species) of ions and water,[16,35−38] while completely omitting structural transport (i.e., transport caused by chemical reactions such as Grotthuss transfer). Simulations with classical force fields also accurately reproduce the density of aqueous salt solutions for a wide range of pressures, temperatures, and salt concentrations,[16,36−38] in sharp contrast to many MLMD and AIMD simulations.[6,28] Earlier works added structural transport to classical force field-based trajectories with a Lattice Monte Carlo postprocessing method.[25,26] This method still requires AIMD simulations to determine the reaction probabilities required for the Lattice Monte Carlo algorithm. In this work, we exploit this separation differently. While the vehicular component of the transferring ion is similarly taken directly from classical MD simulations (thereby ensuring correct vehicular transport and accurate densities and viscosities as a function of temperature, pressure, and salt concentration), the structural contribution is obtained from the difference between simulated and experimentally measured electrical conductivities. The close agreement between classical MD and experimental data for nonreactive mixtures validates the used force fields for vehicular transport,[16,35−38] suggesting that differences for systems with Grotthuss transferring ions mainly arise from the missing structural contribution. Using this insight, we developed a method to estimate Grotthuss transfer rates and ion self-diffusion coefficients without resorting to computationally expensive AIMD or MLMD simulations. Our approach combines classical MD results with a biased random walk model that captures the combined effects of vehicular and structural transport. The parameters of this biased random walk are obtained from differences between electrical conductivities computed from classical MD simulations and available experimental data on electrical conductivities. We mathematically show that correcting classical self-diffusion coefficients from MD for Grotthuss transfer does not require detailed knowledge on reaction properties such as transfer distance or the exact bias in the biased random walk. We show that these properties are required for determining ion lifetimes and indicate how this introduces ambiguity when comparing ion lifetimes in AIMD and MLMD simulations. We demonstrate the method for NaOH(aq), KOH(aq), and HCl(aq) solutions for a broad concentration and temperature range (0−18 mol_{salt}/kg_{water}, 25 and 60 °C). The computed self-diffusion coefficients and ion lifetimes match well with AIMD and MLMD simulations from literature, while requiring only a fraction of the computational cost. Additionally, our simulation results at low concentrations agree with experimental measurements of self-diffusion coefficients at infinite dilution, unlike some results shown in MLMD studies.[30,39] This establishes a

https://doi.org/10.1021/acs.jpcb.5c07132
J. Phys. Chem. B 2026, 130, 1332−1345

practical and broadly applicable route for quantifying proton transport in aqueous solutions without the need for expensive AIMD or MLMD simulations.

The structure of this paper is as follows. The mathematical background and underlying assumptions are discussed in Section 2. The simulation setup and force field selection are presented in Section 3. Section 4 presents and discusses the simulation results, including validation properties such as densities, viscosities, and the self-diffusion coefficients of K^+, Na^+, and Cl^-. Additionally, this section reports OH^- and H_3O^+ lifetimes and self-diffusion coefficients computed with our method. The conclusions are summarized in Section 5.

2. THEORY

Combining a random walk model with classical MD trajectories is possible because Grotthuss transfer events display stochastic behavior similar to random walks,[40,41] as Grotthuss transfer events are (1) rotational invariant, (2) occur at a rate determined by the average OH^- or H_3O^+ lifetimes (τ), and (3) have a jumping distance (Δ_{hop}). These characteristics have already been established in earlier studies,[20,28,40,41] however, for completeness this is also shown in our results section using trajectories obtained from MLIP simulations.[6] Our model relies on two main assumptions: (1) The classical force field captures the vehicular transport of the ions correctly, including all concentration effects. This assumption is justified as classical force fields reproduce vehicular transport of other ions reliably, as shown in earlier studies.[16,36−38] We also confirmed this in our simulations, which reproduce the temperature and salt concentration dependence of the densities, viscosities, and self-diffusion coefficients of K^+, Na^+, Cl^-, and water, consistent with experiments. (2) The trajectory of a particle due to Grotthuss transfer is only self-correlated. There are no cross-correlations with the trajectories of other particles, either ions or water molecules. The vehicular trajectory of a Grotthuss transferring particle is also uncorrelated to the trajectory due to the Grotthuss transfer of the same particle. This assumption enables simplification of the expressions for self-diffusion and electrical conductivity. This provides a new perspective compared to earlier publications, which indicated that the local environment of OH^- and H_3O^+ is very relevant for Grotthuss transfer.[3,4,6,28] References 27, 30 also revealed that the influence of the local environment on Grotthuss transfer changes at higher concentrations. However, such local effects only influence the probability and direction of transfer events taking place on the short time scales. In the long-time limit, we define the correlation between the time signals $\mathbf{a}(t)$ and $\mathbf{b}(t)$, following Helfand:[42]

$$C(\mathbf{a}, \mathbf{b}) \propto \lim_{t\to\infty} \frac{1}{t}\langle(\mathbf{a}(t) - \mathbf{a}(0))\cdot(\mathbf{b}(t) - \mathbf{b}(0))\rangle \quad (1)$$

In this study, $\mathbf{a}(t)$ and $\mathbf{b}(t)$ represent ion coordinates, although the definition is general. The limit $t \to \infty$ in eq 1 means that only long-time effects are captured. The interactions of the microscopic environment may influence the direction of Grotthuss transfer in the short time after transfer events. However, liquids behave chaotically over long times. OH^- or H_3O^+ ions will be reoriented over time due to vehicular transport. This makes the directions of the Grotthuss transfer events random on long time scales. Therefore, the assumption that structural transport of a specific Grotthuss transferring ion is uncorrelated with any trajectory except itself is fully compatible with the relevance of the local environment on how a specific Grotthuss transfer event takes place. The assumption that the Grotthuss transfer trajectory of a particle is only self-correlated is also confirmed with AIMD simulations.[20,40] These AIMD simulations revealed that all other correlations (to other ions or water molecules) can be neglected. Analysis of these AIMD trajectories[20,40] also showed that hydronium and hydroxide are more likely to react with the oxygen atom that belonged to the former OH^- or H_3O^+ molecule, rather than with the oxygen atom of a new water molecule. This means that the structural transport of Grotthuss transfer cannot be modeled with a simple random walk as attempted earlier,[28] and can only be modeled as a biased random walk, which is adjusted to a systematic bias for back-hopping.[43] The relation between a simple random walk and biased random walk model is explained in the following sections. Figure 2 shows how the bias affects the computed ion lifetimes, and compares the biased random walk directly with a simple random walk. With the two aforementioned assumptions, it can be rigorously derived that the experimentally measured electrical conductivity, σ^{exp}, equals the electrical conductivity arising from the superposition of vehicular transport and the biased random walk, σ^{C+BRW}. Here, the superscript ^{C} indicates classical MD trajectories and ^{BRW} refers to the biased random walk. Importantly, we will show that these two transport mechanisms contribute independently and additively to the overall conductivity, so that $\sigma^{C+BRW} = \sigma^C + \sigma^{BRW}$.

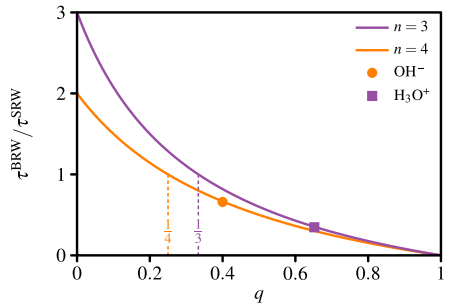

Figure 2. Relation between the Grotthuss transferring ion lifetimes (τ) calculated using a BRM versus a SRW depending on the number of possible reaction directions (n) and the probability of hopping back (q). The dashed lines indicate where there is no bias for back-hopping: $q = 1/n$. Earlier works[20,40] established that OH^- and H_3O^+ are more likely to hop back during a Grotthuss transfer event than expected from a simple random walk. This means that $q > 1/n$, and this figure clearly shows that τ^{BRW} is then smaller than what would be estimated using a SRW. The values of q and n, used in this work, and the resulting τ^{BRW}/τ^{SRW} of hydroxide (orange circle) and hydronium (purple square) are shown as well. The selection of the values of q and n is discussed in Section 4.

2.1. Self-Diffusion Coefficients

The self-diffusion coefficient of species (also valid for an ion) type i (D_{self_i}) is computed using mean squared displacements (MSD) according the Einstein equation:[42,44−46]

$$D_{self_i} = \frac{1}{6N_i}\lim_{t\to\infty}\frac{1}{t}\sum_{k=1}^{N_i}\langle(\mathbf{r}_{k,i}(t) - \mathbf{r}_{k,i}(0))^2\rangle \quad (2)$$

were N_i indicates the number of particles of species i, t is time, and $\mathbf{r}_{k,i}$ is the position of particle k of species i in 3D. In our

https://doi.org/10.1021/acs.jpcb.5c07132
J. Phys. Chem. B 2026, 130, 1332−1345

analysis, the full trajectory consists of vehicular transport and the biased random walk: $\mathbf{r}_{k,i}^{\mathrm{C+BRW}} = \mathbf{r}_{k,i}^{\mathrm{C}} + \mathbf{r}_{k,i}^{\mathrm{BRW}}$. For clarity, we will first analyze the cases of only having vehicular transport ($D_{\mathrm{self}_i}^{\mathrm{C}}$) and only the biased random walk ($D_{\mathrm{self}_i}^{\mathrm{BRW}}$) before considering the combined self-diffusion coefficient $D_{\mathrm{self}_i}^{\mathrm{C+BRW}}$.

The self-diffusion coefficient of the classical vehicular trajectory ($D_{\mathrm{self}_i}^{\mathrm{C}}$) is in basis the same as eq 2, but is computed using the positions from classical MD simulations $\mathbf{r}_{k,i}^{\mathrm{C}}$. These are obtained from MD simulations in a simulation box with periodic boundary conditions. It has been shown that periodic boundary conditions result in an underestimation of the self-diffusion coefficient. Therefore, a finite-size correction $D_{\mathrm{self}}^{\mathrm{FS}}$ has to be added to $D_{\mathrm{self}_i}^{\mathrm{C}}$.[47] The Yeh and Hummer correction was used for the finite-size effects of a cubic simulation box.[47,48] This correction ($D_{\mathrm{self}}^{\mathrm{FS}}$) incorporates the viscosity η that has no finite-size effects in most fluids:[45−51]

$$D_{\mathrm{self}}^{\mathrm{FS}} = \frac{\xi k_{\mathrm{B}} T}{6\pi\eta L} \tag{3}$$

$$\eta = \frac{L^3}{20 k_{\mathrm{B}} T} \lim_{t\to\infty} \frac{1}{t} \left\langle \sum_{\alpha\beta} \left(\int_0^t P_{\alpha\beta}^{\mathrm{OS}}(t')\mathrm{d}t' \right)^2 \right\rangle \tag{4}$$

$$P_{\alpha\beta}^{\mathrm{OS}} = \frac{P_{\alpha\beta} + P_{\beta\alpha}}{2} - \delta_{\alpha\beta}\left(\frac{1}{3}\sum_k P_{kk}\right) \tag{5}$$

where ξ is a dimensionless constant equal to 2.837297, k_{B} is the Boltzmann constant, T is the absolute temperature, L is the simulation box length, and $P_{\alpha\beta}^{\mathrm{OS}}$ is the traceless pressure tensor.[52] $P_{\alpha\beta}^{\mathrm{OS}}$ depends on all 9 stress tensor components ($P_{\alpha\beta}$) and the Kronecker delta ($\delta_{\alpha\beta}$), while $\sum_k P_{kk}$ is the invariant trace of the pressure tensor. Using the maximum available information on the stress tensor components increases the statistical reliability of the computed value of η.[52]

The self-diffusion coefficient of the biased random walk $D_{\mathrm{self}_i}^{\mathrm{BRW}}$ can be determined by using the trajectory of the biased random walk $\mathbf{r}_{k,i}^{\mathrm{BRW}}$ in eq 2. The self-diffusion coefficients of simple and biased random walks have been derived in earlier studies.[40,43] These studies assumed infinite system size, and therefore do not require finite-size corrections. The self-diffusion coefficient of a simple random walk can be described using only two parameters:

$$D_{\mathrm{self}_i}^{\mathrm{SRW}} = \frac{\Delta_{\mathrm{hop}}^2}{6\tau} \tag{6}$$

where τ and Δ_{hop} denote the lifetime of a Grotthuss transferring ion and the average distance it covers during a transfer event, respectively. Chen et al.[19] derived that the self-diffusion coefficient of a random walk with a bias toward hopping back equals that of a simple random walk with a prefactor depending on this bias:

$$D_{\mathrm{self}_i}^{\mathrm{BRW}} = \frac{n - nq}{n + nq - 2} D_{\mathrm{self}_i}^{\mathrm{SRW}} \tag{7}$$

This prefactor contains two parameters, the number of possible directions Grotthuss transfer (n) and the probability of hopping back (q). One would expect an unbiased, simple random walk to have a probability $1/n$ into any of the n reaction directions. The bias toward hopping back with probability q only leaves a probability of $1 - q$ into the other directions, which we assume to each have equal probability $p = (1 - q)/(1 - n)$. The prefactor is 1 when $q = 1/n$, so eqs 6 and 7 are identical if there is no back-hopping bias.

The self-diffusion coefficient of the combined transport $D_{\mathrm{self}_i}^{\mathrm{C+BRW}}$ depends on the sum of the vehicular and structural trajectories, $\mathbf{r}_{k,i}^{\mathrm{C+BRW}} = \mathbf{r}_{k,i}^{\mathrm{C}} + \mathbf{r}_{k,i}^{\mathrm{BRW}}$:

$$D_{\mathrm{self}_i}^{\mathrm{C+BRW}} = \frac{1}{6N_i} \lim_{t\to\infty} \frac{1}{t} \sum_{k=1}^{N_i} \langle ((\mathbf{r}_{k,i}^{\mathrm{C}}(t) + \mathbf{r}_{k,i}^{\mathrm{BRW}}(t)) - (\mathbf{r}_{k,i}^{\mathrm{C}}(0) + \mathbf{r}_{k,i}^{\mathrm{BRW}}(0)))^2 \rangle + D_{\mathrm{self}}^{\mathrm{FS}} \tag{8}$$

$$= \frac{1}{6N_i} \lim_{t\to\infty} \frac{1}{t} \sum_{k=1}^{N_i} \langle (\mathbf{r}_{k,i}^{\mathrm{C}}(t) - \mathbf{r}_{k,i}^{\mathrm{C}}(0))^2 + (\mathbf{r}_{k,i}^{\mathrm{BRW}}(t) - \mathbf{r}_{k,i}^{\mathrm{BRW}}(0))^2 + 2(\mathbf{r}_{k,i}^{\mathrm{C}}(t) - \mathbf{r}_{k,i}^{\mathrm{C}}(0))\cdot(\mathbf{r}_{k,i}^{\mathrm{BRW}}(t) - \mathbf{r}_{k,i}^{\mathrm{BRW}}(0)) \rangle + D_{\mathrm{self}}^{\mathrm{FS}} \tag{9}$$

The finite-size correction ($D_{\mathrm{self}}^{\mathrm{FS}}$) was added to $D_{\mathrm{self}_i}^{\mathrm{C+BRW}}$ as vehicular transport component is computed using classical MD with periodic boundary conditions (eq 3). The next step is using the second main assumption, which states that the structural (Grotthuss) transport of an ion is independent of the vehicular transport of that ion. In other words, the biased random walk of molecule k is uncorrelated with the classical trajectory of the same molecule. This means that the cross-correlation term

$$\lim_{t\to\infty} \frac{1}{t} \sum_{k=1}^{N_i} \langle (\mathbf{r}_{k,i}^{\mathrm{C}}(t) - \mathbf{r}_{k,i}^{\mathrm{C}}(0))\cdot(\mathbf{r}_{k,i}^{\mathrm{BRW}}(t) - \mathbf{r}_{k,i}^{\mathrm{BRW}}(0)) \rangle = 0 \tag{10}$$

can be dropped, and the overall equation for $D_{\mathrm{self}_i}^{\mathrm{C+BRW}}$ can be split into two independent terms for the vehicular trajectory and the biased random walk:

$$D_{\mathrm{self}_i}^{\mathrm{C+BRW}} = \frac{1}{6N_i} \lim_{t\to\infty} \frac{1}{t} \sum_{k=1}^{N_i} \langle (\mathbf{r}_{k,i}^{\mathrm{C}}(t) - \mathbf{r}_{k,i}^{\mathrm{C}}(0))^2 \rangle + D_{\mathrm{self}}^{\mathrm{FS}} + \frac{1}{6N_i} \lim_{t\to\infty} \frac{1}{t} \sum_{k=1}^{N_i} \langle (\mathbf{r}_{k,i}^{\mathrm{BRW}}(t) - \mathbf{r}_{k,i}^{\mathrm{BRW}}(0))^2 \rangle \tag{11}$$

$$= D_{\mathrm{self}_i}^{\mathrm{C}} + D_{\mathrm{self}_i}^{\mathrm{BRW}} \tag{12}$$

Substituting eq 7 into eq 12 retrieves the combined self-diffusion coefficient:

$$D_{\mathrm{self}_i}^{\mathrm{C+BRW}} = D_{\mathrm{self}_i}^{\mathrm{C}} + \frac{n - nq}{n + nq - 2} \frac{\Delta_{\mathrm{hop}}^2}{6\tau} \tag{13}$$

This shows that $D_{\mathrm{self}_i}^{\mathrm{C+BRW}}$ can be calculated by adding the structural transport to simulation results computed with classical MD. For very large τ, i.e., for molecules that rarely or not at all perform Grotthuss hopping, the contribution from the biased random walk becomes negligible, and eq 13 simplifies to $D_{\mathrm{self}_i}^{\mathrm{C+BRW}} = D_{\mathrm{self}_i}^{\mathrm{C}}$.

2.2. Electrical Conductivity

The electrical conductivity (σ) can be computed with either the Nernst−Einstein[16,17] or the Einstein-Helfand[16,17] equations. We applied the Einstein-Helfand equation because the

https://doi.org/10.1021/acs.jpcb.5c07132
J. Phys. Chem. B 2026, 130, 1332−1345

often used Nernst−Einstein equation does not incorporate ion−ion correlation effects, which are relevant beyond infinite dilution.[16,17] The Einstein-Helfand equation does not (or only little) suffer from finite-size effects.[16,53] Instead of sampling the mean squared displacement of the charge center of the simulation box, the electrical conductivity can be fully expressed using the Onsager coefficients:[16,17,44]

$$\sigma = \frac{e^2 z^2 N_{\text{tot}}}{k_B T V}(\Lambda_{++} - 2\Lambda_{+-} + \Lambda_{--}) \tag{14}$$

$$\Lambda_{i,j} = \frac{1}{6N_{\text{tot}}} \lim_{t\to\infty} \frac{1}{t} \sum_{k=1}^{N_i} \sum_{l=1}^{N_j} \langle (\mathbf{r}_{k,i}(t) - \mathbf{r}_{k,i}(0)) \cdot (\mathbf{r}_{l,j}(t) - \mathbf{r}_{l,j}(0)) \rangle \tag{15}$$

where e is the electron charge and z is the absolute value of the unit charge of the indicated ions. $\Lambda_{i,j}$ are the Onsager coefficients between the cations (+) and anions (−), in which N_{tot} is the total number of particles (molecules, ions) in the simulation box, and N_i and N_j are the total numbers of particles of species i and j, respectively. Even if scaled ion charges are used in the force field, for computing electrical conductivities full charges must be used in eq 14.[16] Hence, z^2 is set to 1 in all postprocessing steps, as only consider monovalent ions are considered.

We require two definitions for electrical conductivity. The first is the electrical conductivity determined using vehicular trajectories as captured from classical MD trajectories (σ^{C}). This is computed from eq 14 for which the Onsager coefficients ($\Lambda_{i,j}^{\text{C}}$) are calculated from vehicular trajectories retrieved from classical MD simulations (using the trajectory of $\mathbf{r}_{k,i}^{\text{C}}$). The second is the electrical conductivity of the combined vehicular and structural transport ($\sigma^{\text{C+BRW}}$), depending on Onsager coefficients ($\Lambda_{i,j}^{\text{C+BRW}}$), calculated from both the classically computed vehicular trajectories and the biased random walk, $\mathbf{r}_{k,i}^{\text{C+BRW}} = \mathbf{r}_{k,i}^{\text{C}} + \mathbf{r}_{k,i}^{\text{BRW}}$. Similarly to self-diffusion coefficients, the combined Onsager coefficient $\Lambda_{i,j}^{\text{C+BRW}}$ can be split into a vehicular part from classical molecular dynamics $\Lambda_{i,j}^{\text{C}}$ and the structural transport part modeled with a biased random walk $\Lambda_{i,j}^{\text{BRW}}$. For this, we again rely on the assumption that there is no correlational between the vehicular transport and the biased random walk. This means that

$$\lim_{t\to\infty} \frac{1}{t} \sum_{k=1}^{N_i} \sum_{l=1}^{N_j} \langle (\mathbf{r}_{k,i}^{\text{C}}(t) - \mathbf{r}_{k,i}^{\text{C}}(0)) \cdot (\mathbf{r}_{l,j}^{\text{BRW}}(t) - \mathbf{r}_{l,j}^{\text{BRW}}(0)) \rangle \approx 0 \tag{16}$$

$$\lim_{t\to\infty} \frac{1}{t} \sum_{k=1}^{N_i} \sum_{l=1}^{N_j} \langle (\mathbf{r}_{k,i}^{\text{BRW}}(t) - \mathbf{r}_{k,i}^{\text{BRW}}(0)) \cdot (\mathbf{r}_{l,j}^{\text{C}}(t) - \mathbf{r}_{l,j}^{\text{C}}(0)) \rangle \approx 0 \tag{17}$$

With this, we can derive that

$$\begin{aligned}\Lambda_{i,j}^{\text{C+BRW}} = \frac{1}{6N_{\text{tot}}} \lim_{t\to\infty} \frac{1}{t} \sum_{k=1}^{N_i} \sum_{l=1}^{N_j} \langle ((\mathbf{r}_{k,i}^{\text{C}}(t) + \mathbf{r}_{k,i}^{\text{BRW}}(t)) \\ - (\mathbf{r}_{k,i}^{\text{C}}(0) + \mathbf{r}_{k,i}^{\text{BRW}}(0)))((\mathbf{r}_{l,j}^{\text{C}}(t) + \mathbf{r}_{l,j}^{\text{BRW}}(t)) \\ - (\mathbf{r}_{l,j}^{\text{C}}(0) + \mathbf{r}_{l,j}^{\text{BRW}}(0)))\rangle\end{aligned} \tag{18}$$

$$\begin{aligned}= \frac{1}{6N_{\text{tot}}} \lim_{t\to\infty} \frac{1}{t} \sum_{k=1}^{N_i} \sum_{l=1}^{N_j} \langle (\mathbf{r}_{k,i}^{\text{C}}(t) - \mathbf{r}_{k,i}^{\text{C}}(0))(\mathbf{r}_{l,j}^{\text{C}}(t) - \mathbf{r}_{l,j}^{\text{C}}(0)) \\ + (\mathbf{r}_{k,i}^{\text{C}}(t) - \mathbf{r}_{k,i}^{\text{C}}(0))(\mathbf{r}_{l,j}^{\text{BRW}}(t) - \mathbf{r}_{l,j}^{\text{BRW}}(0)) \\ + (\mathbf{r}_{k,i}^{\text{BRW}}(t) - \mathbf{r}_{k,i}^{\text{BRW}}(0))(\mathbf{r}_{l,j}^{\text{BRW}}(t) - \mathbf{r}_{l,j}^{\text{BRW}}(0)) \\ + (\mathbf{r}_{k,i}^{\text{BRW}}(t) - \mathbf{r}_{k,i}^{\text{BRW}}(0))(\mathbf{r}_{l,j}^{\text{C}}(t) - \mathbf{r}_{l,j}^{\text{C}}(0))\rangle\end{aligned} \tag{19}$$

$$\begin{aligned}= \frac{1}{6N_{\text{tot}}} \lim_{t\to\infty} \frac{1}{t} \sum_{k=1}^{N_i} \sum_{l=1}^{N_j} \langle (\mathbf{r}_{k,i}^{\text{C}}(t) - \mathbf{r}_{k,i}^{\text{C}}(0))(\mathbf{r}_{l,j}^{\text{C}}(t) - \mathbf{r}_{l,j}^{\text{C}}(0))\rangle \\ + \frac{1}{6N_{\text{tot}}} \lim_{t\to\infty} \frac{1}{t} \sum_{k=1}^{N_i} \sum_{l=1}^{N_j} \langle (\mathbf{r}_{k,i}^{\text{BRW}}(t) - \mathbf{r}_{k,i}^{\text{BRW}}(0)) \\ (\mathbf{r}_{l,j}^{\text{BRW}}(t) - \mathbf{r}_{l,j}^{\text{BRW}}(0))\rangle\end{aligned} \tag{20}$$

$$= \Lambda_{i,j}^{\text{C}} + \Lambda_{i,j}^{\text{BRW}} \tag{21}$$

This means that the structural transport (modeled with the biased random walk) is independent of the vehicular transport (computed with classical MD). This implies that the effect of structural transport can be entirely accounted for in a postprocessing stage of a classical MD trajectory, without the need to explicitly incorporate the biased random walk into the MD simulation itself. As established by Fischer et al.,[40] other ions do not correlated with the biased random walk of an specific ion. This means that the only nonzero contribution to the Onsager coefficient is from an ion with itself, $\Lambda_{i,j=i}^{\text{BRW}}$, to which only a specific ion to itself ($l = k$) contributes. Therefore, $\Lambda_{i,j\neq i}^{\text{BRW}} = 0$, and $\Lambda_{i,j=i}^{\text{BRW}}$ can be further simplified using the aforementioned approximation if $l \neq k$. We split the double summations into diagonal contributions ($l = k$), and into upper and lower triangle contributions, with $l < k$ and $l > k$, respectively:

$$\Lambda_{i,i}^{\text{BRW}} = \frac{1}{6N_{\text{tot}}} \lim_{t\to\infty} \frac{1}{t} \sum_{k=1}^{N_i} \sum_{l=1}^{N_i} \left\langle (\mathbf{r}_{k,i}^{\text{BRW}}(t) - \mathbf{r}_{k,i}^{\text{BRW}}(0)) \cdot (\mathbf{r}_{l,i}^{\text{BRW}}(t) - \mathbf{r}_{l,i}^{\text{BRW}}(0)) \right\rangle \tag{22}$$

$$\begin{aligned}= \frac{1}{6N_{\text{tot}}} \lim_{t\to\infty} \frac{1}{t} \sum_{k=1}^{N_i} \sum_{l=1}^{k-1} \left\langle (\mathbf{r}_{k,i}^{\text{BRW}}(t) - \mathbf{r}_{k,i}^{\text{BRW}}(0)) \cdot (\mathbf{r}_{l,i}^{\text{BRW}}(t) - \mathbf{r}_{l,i}^{\text{BRW}}(0)) \right\rangle + \frac{1}{6N_{\text{tot}}} \lim_{t\to\infty} \frac{1}{t} \\ \sum_{k=1}^{N_i} \sum_{l=k}^{k} \left\langle (\mathbf{r}_{k,i}^{\text{BRW}}(t) - \mathbf{r}_{k,i}^{\text{BRW}}(0)) \cdot (\mathbf{r}_{l,i}^{\text{BRW}}(t) - \mathbf{r}_{l,i}^{\text{BRW}}(0)) \right\rangle \\ + \frac{1}{6N_{\text{tot}}} \lim_{t\to\infty} \frac{1}{t} \sum_{k=1}^{N_i} \sum_{l=k+1}^{N_i} \left\langle (\mathbf{r}_{k,i}^{\text{BRW}}(t) - \mathbf{r}_{k,i}^{\text{BRW}}(0)) \cdot (\mathbf{r}_{l,i}^{\text{BRW}}(t) - \mathbf{r}_{l,i}^{\text{BRW}}(0)) \right\rangle\end{aligned} \tag{23}$$

$$= \frac{1}{6N_{\text{tot}}} \lim_{t\to\infty} \frac{1}{t} \sum_{k=1}^{N_i} \left\langle (\mathbf{r}_{k,i}^{\text{BRW}}(t) - \mathbf{r}_{k,i}^{\text{BRW}}(0))^2 \right\rangle \tag{24}$$

https://doi.org/10.1021/acs.jpcb.5c07132
J. Phys. Chem. B 2026, 130, 1332−1345

The final expression (eq 24) is the self-diffusion coefficient of the biased random walk scaled by the molar ratio between N_{tot} and N_i: $\Lambda_{i,i}^{BRW} = \frac{N_i}{N_{tot}} D_{self_i}^{BRW}$. Equivalent to the self-diffusion coefficients, the bias in the random walk is compensated for by using probabilities q and n. Therefore, the Onsager coefficient contribution of the Grotthuss transferring ions follows from

$$\Lambda_{i,i}^{BRW} = \frac{N_i}{N_{tot}} \frac{n - nq}{n + nq - 2} \frac{\Delta_{hop}^2}{6\tau} \tag{25}$$

Inserting this expression (eq 25) into eq 14 yields the electrical conductivity of the combined vehicular and structural transport:

$$\sigma^{C+BRW} = \frac{e^2 z^2 N_{tot}}{k_B T V} (\Lambda_{++}^{C} + \Lambda_{++}^{BRW} - 2\Lambda_{+-}^{C} + \Lambda_{--}^{C} + \Lambda_{--}^{BRW}) \tag{26}$$

All investigated mixtures only contain a single ion species that undergoes Grotthuss transfer events: for NaOH(aq) and KOH(aq) this is OH^- and for HCl(aq) this is H_3O^+. The ion species that do not undergo Grotthuss transfer (K^+, Na^+, and Cl^-) have an infinitely long ion lifetime. The Onsager coefficient of the biased random walk is 0 in this limit, and only the contribution of the Grotthuss transferring ion has to be considered in eq 26. From here on, the Grotthuss-transferring ion species will be indicated with subscript $_{Grott\text{-}ion}$, as the exact type (OH^- or H_3O^+) does not matter for the expression for the electrical conductivity. Equation 21 shows that one can split the Onsager coefficient of a Grotthuss transferring ion into the classical contribution and that of the biased random walk. This leads to

$$\sigma^{C+BRW} = \frac{e^2 z^2 N_{tot}}{k_B T V} (\Lambda_{++}^{C} - 2\Lambda_{+-}^{C} + \Lambda_{--}^{C} + \Lambda_{Grott\text{-}ion,Grott\text{-}ion}^{BRW}) \tag{27}$$

$$= \sigma^{C} + \frac{e^2 z^2 N_{Grott\text{-}ion}}{k_B T V} \frac{n - nq}{n + nq - 2} \frac{\Delta_{hop}^2}{6\tau} \tag{28}$$

for which $N_{Grott\text{-}ion}$ are the number of OH^- or H_3O^+ ions in the solution. Using our assumptions, σ^{C+BRW} equals the experimental electrical conductivity, including both the vehicular and structural transport. From this, it is possible to extract the biased random walk contribution of the Onsager coefficient in terms of difference between σ^{exp} and σ^{C}:

$$\Lambda_{Grott\text{-}ion,Grott\text{-}ion}^{BRW} = \frac{k_B T V}{N_{tot} e^2 z^2} (\sigma^{exp} - \sigma^{C}) \tag{29}$$

It is also possible to compute the Grotthuss transferring ion lifetime τ from the difference between the experimentally measured conductivities (σ^{exp}) and the electrical conductivity computed with classical MD (σ^{C}):

$$\tau = \frac{n - nq}{n + nq - 2} \frac{\Delta_{hop}^2}{6} \frac{e^2 z^2 N_{Grott\text{-}ion}}{k_B T V (\sigma^{exp} - \sigma^{C})} \tag{30}$$

This enables us to investigate how the bias in the random walk influences the Grotthuss transferring ion lifetimes τ. Figure 2 shows that increasing the back-hopping probability q reduces τ, leading to shorter lifetimes compared to a simple random walk (SRW). A higher tendency for back-hopping decreases the mean squared displacement, resulting in less efficient transport. The ratio τ^{BRW}/τ^{SRW} in Figure 2 clearly illustrates this trend as a function of q. Substituting τ from eq 30 into eq 13 shows that the self-diffusion coefficients of H_3O^+ and OH^- ($D_{self,\ Grott\text{-}ion}^{C+BRW}$) are independent of the Grotthuss transfer distance Δ_{hop} and the back-hopping bias:

$$D_{self,Grott\text{-}ion}^{C+BRW} = D_{self,Grott\text{-}ion}^{C} + \frac{k_B T V (\sigma^{exp} - \sigma^{C})}{e^2 z^2 N_{Grott\text{-}ion}} \tag{31}$$

Therefore, $D_{self,\ Grott\text{-}ion}^{C+BRW}$ is linearly dependent on the difference between experimental and simulated electrical conductivities, without any dependence on the mechanism of the Grotthuss transfer. Due to the back-hopping nature of Grotthuss transfer, it is often ambiguous whether a transfer event should be considered complete, since protons may rapidly hop forward and backward between neighboring sites. This ambiguity complicates the extraction of consistent lifetimes of Grotthuss transferring ions from AIMD or MLMD trajectories. As a result, different methods used to compute Grotthuss transferring ion lifetimes from AIMD and MLMD simulations[3,4,6,20,27,28,39,40] yield significant variations in the reported lifetimes, ranging from 1.3 to 4.1 ps[6,39] for OH^- an 0.5 ps to 1.5 ps[28,40] for H_3O^+, all at comparable low concentrations and ambient conditions. The precise definition what constitutes a Grotthuss transfer event affects not only the lifetimes but also the characteristics of the biased random walk. For instance, a method that only registers Grotthuss transfer when a very stable OH^- is converted into a very stable H_2O will obtain a larger value for τ than a method with less strict requirements. The stricter approach will also report a lower back-hopping probability q, as fewer transient forward−backward fluctuations are counted as transfer events. Such issues do not affect macroscopic transport properties like ion self-diffusion coefficients and electrical conductivities, as shown in eq 31. Both $D_{self,\ Grott\text{-}ion}^{C+BRW}$ and σ^{C+BRW} are computed from the net movement of ions and are insensitive to how individual transfer events are counted. This makes $D_{self,\ Grott\text{-}ion}^{C+BRW}$ and σ^{C+BRW} more reliable for comparing simulation techniques than τ.

2.3. Toward Maxwell−Stefan Diffusion Coefficients

Maxwell-Steffan diffusion coefficients between water and ion can be computed with the Onsager coefficients described above.[54,55] Following the methodology described by Krishna et al.,[54,55] one needs to determine the Δ matrix. Our notation is consistent with the earlier equations; Δ^{C} is computed using classical trajectories, Δ^{BRW} is computed from the biased random walk, and Δ^{C+BRW} is determined using the combined trajectories. For an n component mixture, we selected the last species to be Grotthuss transferring, as this simplifies the equations. The elements of the Δ matrix are then:[54,55]

$$\Delta_{ij}^{C+BRW} = (N_{tot} - N_i)\left(\frac{\Lambda_{ij}^{C+BRW}}{N_j} - \frac{\Lambda_{in}^{C+BRW}}{N_n}\right) - N_i \sum_{k=1,k\neq i}^{k=n} \left(\frac{\Lambda_{kj}^{C+BRW}}{N_j} - \frac{\Lambda_{kn}^{C+BRW}}{N_n}\right) \tag{32}$$

$$= \Delta_{ij}^{C} + \frac{\Lambda_{Grott\text{-}ion,Grott\text{-}ion}^{BRW}}{N_{Grott\text{-}ion}} N_i \tag{33}$$

https://doi.org/10.1021/acs.jpcb.5c07132
J. Phys. Chem. B 2026, 130, 1332−1345

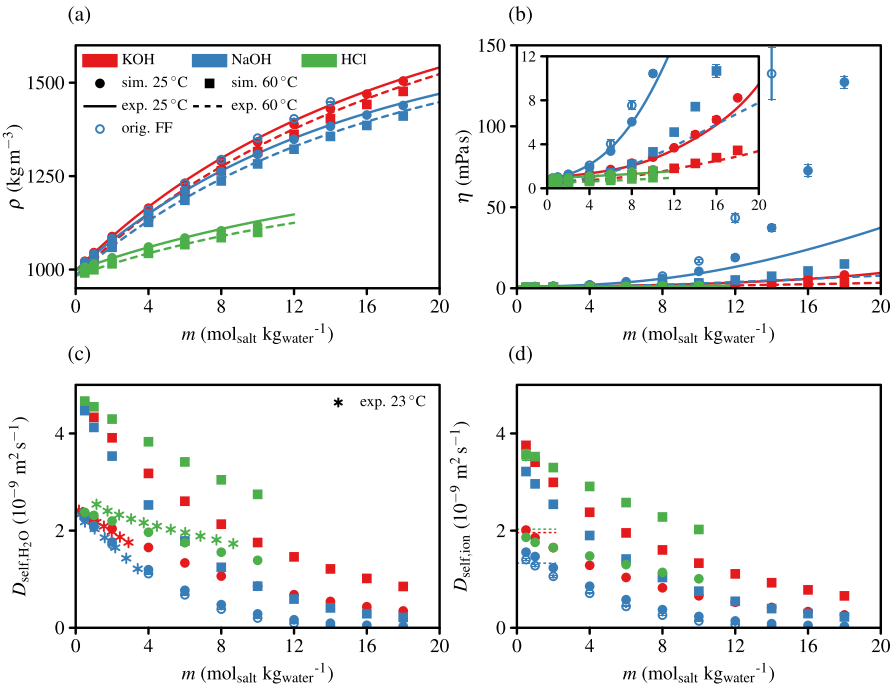

Figure 3. (a) Densities, (b) viscosities, (c) water self-diffusion coefficients, and (d) self-diffusion coefficients of Na^+ K^+, and Cl^-. The viscosities and water and ion self-diffusion coefficients indicate how well vehicular transport is captured in these classical MD simulations. The results for KOH(aq) are indicated in red, NaOH(aq) in blue, and HCl(aq) in green. Circles indicate simulation results at 25 °C and squares indicate those at 60 °C. Simulations of NaOH(aq) at 25 °C performed with the original FF[36,37] are shown with open blue circles. All simulation results are shown with error bars that are twice the standard deviation. Error bars are only visible in the most viscous mixtures, as the 100 ns provide very consistent results. The continuous lines are experimental fit curves.[66] (c) The asterisks are experimental results at 23 °C.[67] (d) The dashed horizontal lines at low concentration show experimental self-diffusion coefficients of the non-Grotthuss transferring ions at infinite dilution.[18]

for rows and columns $i, j = 1, 2, \cdots, n-1$, with n being the total number of species in the system. Note that we used that species n is the only Grotthuss transferring component in between eqs 32 and 33. Instead of describing the Δ matrix element−wise, it is convenient to construct the full matrix form:

$$\Delta^{C+BRW} = \Delta^{C} + \frac{\Lambda^{BRW}_{Grott\text{-}ion,Grott\text{-}ion}}{N_{Grott\text{-}ion}}\mathbf{N}\mathbf{1}^{T} \tag{34}$$

$$= \Delta^{C} + \frac{k_B T V}{N_{Grott\text{-}ion} N_{tot} e^2 z^2}(\sigma^{exp} - \sigma^{C})\mathbf{N}\mathbf{1}^{T} \tag{35}$$

where $\mathbf{N}$ is the column vector whose entries are N_i for $i = 1, \cdots, n-1$, and $\mathbf{1}^T$ is the transpose of the vector of ones. The outer product between $\mathbf{N}$ and $\mathbf{1}^T$ results in a row-constant matrix, which appropriately corrects for the biased random walk. The term Δ^{C+BRW} can be used directly to compute Maxwell-Stefan diffusion coefficients, as described in detail by Krishna et al.[54,55] Fully deriving the Maxwell-Stefan diffusion coefficients from this involves inverting the matrix Δ^{C+BRW}, which is straightforward, however causes all components to depend on all elements in Δ^{C+BRW}. Therefore, all Maxwell-Stefan diffusion coefficients are influenced by the biased random walk, and thus the structural transport of the Grotthuss transferring species.

3. COMPUTATIONAL DETAILS

Classical force field-based MD simulations were performed using the LAMMPS[56,57] software with the OCTP plugin.[44] This plugin is used to compute the relevant transport coefficients (η, $D^C_{self,i}$, $\Lambda^C_{i,j}$). The simulations of NaOH(aq), KOH(aq), and HCl(aq) are performed at 1 bar and at 25 and 60 °C using a cubic simulation box with periodic boundary conditions in all directions. The classical, nonpolarizable, and rigid TIP4P/2005 water model,[35] along with the Madrid-Transport family of ion force fields,[36−38] was selected because these have shown reliable predictions of both thermodynamic and transport properties of water and ions.[16,35−38] The simulations of NaOH(aq) and KOH(aq) contained 1100 water molecules and the appropriate number of ion-pairs (for the investigated molalities 0.5, 1, 2, 4, 6, 8, 10, 12, 14, 16, and 18 mol salt per kg water) and were modeled with the classical Madrid-Transport[37] and the DFF/OH^-[36] force fields. force field showed significant overestimation of densities and viscosities at high concentrations. This is clearly shown in Figure 3, and is further investigated in Section 4. This issue is mitigated by increasing the Lennard-Jones radius between Na^+ and O_{water} by 10%. Increasing this radius increases the diameter of the hydration around Na^+ ions, which improves the likelihood of Na^+ escaping its hydration. This, in turn, increases the mobility of both Na^+ and H_2O at high concentrations. Results of the original NaOH(aq) force field are reported as well for comparison.

Classical MD simulations of HCl(aq) were performed using the appropriate number of ion-pairs (for the investigated molalities 0.5, 1, 2, 4, 6, 8, and 10 mol HCl(aq) per kg water). The number of water molecules is 1100 minus the number of ion pairs in the system. This accounts for every mol HCl(aq) forming a H_3O^+ by combining H^+ with a water molecule, since the acidified Madrid-Transport force field[38] models H_3O^+ instead of H^+. All initial simulation boxes were prepared using PACKMOL[58] and FFTOOL.[59] The simulations used the SHAKE[60] algorithm to ensure the rigid shape of the H_2O,

https://doi.org/10.1021/acs.jpcb.5c07132
J. Phys. Chem. B 2026, 130, 1332−1345

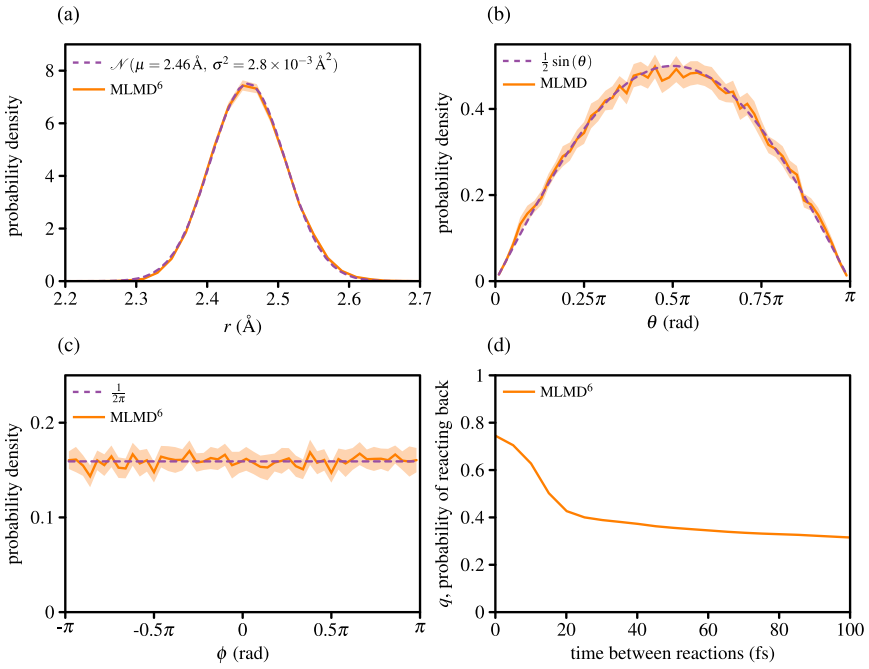

Figure 4. (a–c) Probability density distributions of OH^- Grotthuss transfer steps. The average distance Δ_{hop} = 2.46 Å, and the angles θ and ϕ conform to the sine and uniform distributions, respectively. (d) Probability of reacting back with the oxygen atom that was the former OH^- as a function of the minimal time between Grotthuss transfer of OH^-. The trajectories analyzed here are taken from ref 6.

OH^-, and H_3O^+ molecules. The Lennard-Jones and short-range electrostatic interactions were cut off at 10 Å, and analytical tail corrections for energy and pressure were applied. Long-range electrostatics were modeled with a particle–particle-particle mesh (PPPM)[61] with a 10^{-5} relative error. The velocity-Verlet integrator[62] had a time step of 2 fs and the Nosé-Hoover thermostat and barostat[63,64] were set with a 0.1 and 1 ps coupling constant, respectively. All simulation settings, system sizes and force field parameters are also tabulated in the Supporting Information.

4. RESULTS AND DISCUSSION

While the accuracy of the Madrid-Transport force fields for computing transport properties has been demonstrated in earlier studies,[36−38] these investigations were mostly limited to narrow concentration and temperature ranges. The densities, viscosities, and self-diffusion coefficients of H_2O, together with those of K^+, Na^+, and Cl^-, at the concentrations and temperatures simulated in this study are shown in Figure 3. This figure shows that these force fields also predict these properties accurately at high concentrations. The KOH(aq) force field of ref 36. was only validated up to 8 mol salt per kg water during its development.[36] In Figure 3a,b it is show that this force field results in excellent agreement for density and viscosity properties, even at concentrations as high as 18 mol salt per kg water, without initiating crystallization.

The NaOH(aq) force field of ref 36. was developed with the same method and for the same concentration range as KOH(aq). Significant deviations between simulations and experiments are observed for density at concentrations above 6 mol_{salt} kg_{water}^{-1}, and for viscosity above 8 mol_{salt} kg_{water}^{-1}. Densities of NaOH(aq) are predicted more accurately for all investigated molalities by the recently proposed Madrid-2019-compatible ion force field for OH^-,[65] which was not considered in this paper. However, viscosities are overestimated even more by the force field of ref 65 than the NaOH(aq) force field of ref 36. This results in less ion mobility as well, which is critical for the present study. Because this OH^- force field does not perform any better for KOH(aq) mixtures than the Madrid-Transport force field, we have adjusted the Madrid-Transport NaOH(aq) itself, tweaking it to better perform at higher concentrations. An increase of 10% in the Lennard-Jones radius between Na^+ and O_{water} improved the hydration of Na^+, and therefore the mobility of both Na^+ and H_2O at high concentrations. The improved NaOH(aq) force field shows excellent agreement with experimental density measurements, but still shows deviations in viscosity above 12 mol_{salt} kg_{water}^{-1}. The relative small size of Na^+ (compared to other ions) may be the origin of these issues. The typically short sodium-water distances result in strong electrostatic interactions, which causes stronger polarizability effects in water molecules than for other ions. As the rigid molecule TIP4P/2005 and the Madrid-Transport force fields do not include polarizability effects, it may not be possible to capture the effects of short sodium-water distances accurately. We will not investigate this further, as the NaOH(aq) force field shows excellent agreement with experimental data for densities and viscosities at lower concentrations. Later in this section, it will be shown that there are only minor differences between the OH^- and H_3O^+ lifetimes and self-diffusion coefficients computed from the original and adjusted NaOH(aq) force field.

The HCl(aq) force field has been introduced in a paper by Vega and co-workers.[38] These authors developed a force field for H_3O^+ compatible with the Madrid-2019 ion force fields for which charges are scaled by 0.85. In the same publication, a Madrid-Transport compatible force field for H_3O^+ (with a 0.75 charge scaling) was also listed in the Supporting Information, together with results for density and viscosity.[38] Figure 3 shows that the HCl(aq) force field performs very well for the modeled concentration range for both densities and viscosities. The NaOH(aq) and KOH(aq) force fields also show excellent agreement with the concentration dependence of the water

https://doi.org/10.1021/acs.jpcb.5c07132
J. Phys. Chem. B 2026, 130, 1332−1345

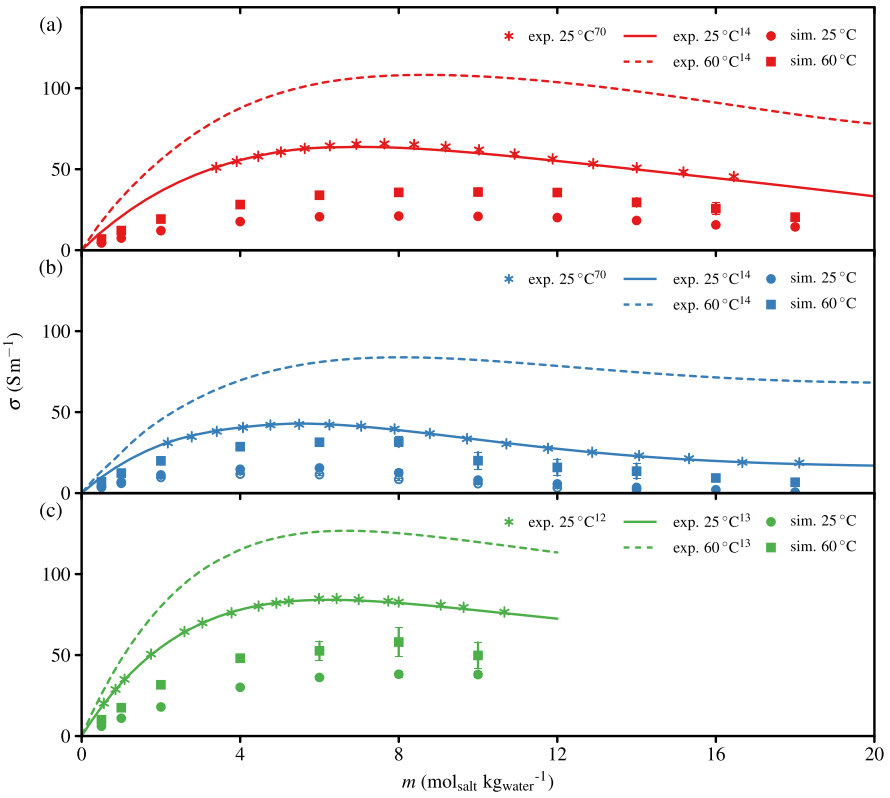

Figure 5. Electrical conductivities of (a) KOH(aq), (b) NaOH(aq), and (c) HCl(aq) at 25 and 60 °C. The curves indicate fits through experimental data,[13,14] and the asterisks are experimental measurements.[12,70] The difference between electrical conductivities computed with classical MD simulations and the experimental value at the same concentration and temperature is used to determine the Grotthuss transferring ion lifetimes and self-diffusion coefficient. (b) The results of the original NaOH(aq) force field at 25 °C are shown as well using open circles.

self-diffusion coefficients found in experiments. Figure 3c shows that the simulated water self-diffusion coefficient is slightly below the experimental data, but the slope of the experimental data matches the simulation results, indicating that the salt concentration dependence of self-diffusion coefficient of water is captured correctly. The self-diffusion coefficient of Cl^- at infinite dilution computed from the classical MD simulations is also close to experimental results. Overall, the recently introduced force field for HCl(aq)[38] shows excellent behavior and integrates well with already existing Madrid-Transport force fields.

It is clear from eq 31 that the self-diffusion coefficients of OH^- and H_3O^+ are independent of the Grotthuss transfer distance Δ_{hop}, and the back-hopping bias q and the average number of possible reaction directions n. These properties are required for determining the ion lifetimes τ with eq 30. To determine these properties, one requires a method that can accurately simulate the Grotthuss transfer process, which can be AIMD or MLMD simulations. MLMD trajectories from Lagerweij et al.[6] have been analyzed to derive these microscopic properties of Grotthuss transfer. Figure 4 shows the probability distribution function of the reaction hopping vectors in spherical coordinates. The probability distribution of the radial distance traveled during Grotthuss transfer of OH^- is used to determine the hopping distance Δ_{hop} = 2.46 Å. The steep normal distribution indicates that the hopping distance is very constant, with a standard deviation of ca. 0.2 Å. This low standard deviation is noteworthy, as the analyzed trajectories were take from simulations at multiple temperatures and densities. Earlier studies[24,40,68] also showed that Δ_{hop} depends very little on temperature, concentration or mixtures. AIMD simulations proton transfer in nonaqueous mixtures resulted in hopping distances of approximately 2.5 Å as well.[68] Sebastiani and co-workers[24] determined that Grotthuss transfer energy barriers vanish when the O−O distance is below 2.44 Å, and Fischer et al.[40] reported that for H_3O^+ Δ_{hop} equals 2.5 Å. Therefore, in this work Δ_{hop} equals 2.46 Å for both OH^- and H_3O^+. Besides deriving Δ_{hop} from AIMD or MLMD simulations, one could also determine it intuitively. Δ_{hop} should be the O−O distance of a strong hydrogen bond, as Grotthuss transfer uses these bonds to deliver a proton to another molecule. Studies into hydrogen bonding have revealed that the strongest hydrogen bond from water to water has an O−O distance of around 2.6 Å.[69] However, Grotthuss transfer involves hydronium or hydroxide and water, for which the strongest hydrogen bond is slightly shorter.[24] This causes this small difference between the hydrogen bond distance between water molecules or between water and OH^- and H_3O^+. The sine distribution of the angle θ in Figure 4b and the uniform distribution of the angle ϕ in Figure 4c indicate that the hopping process is isotropic, meaning that the orientation of the hopping vectors is random on a spherical shell with radius Δ_{hop}. This isotropy is expected for Grotthuss transfer, as it involves breaking and forming hydrogen bonds of molecules with random orientations.

The probability of H_3O^+ for hopping back ($q_{H_3O^+}$) as well as the number of possible reaction directions ($n_{H_3O^+}$) is investigated by Fischer et al.[20,40] The results of that study, $q_{H_3O^+}$ = 0.652 and $n_{H_3O^+}$ = 3, are implemented in our analysis. The possible number of reaction directions of H_3O^+ is

https://doi.org/10.1021/acs.jpcb.5c07132
J. Phys. Chem. B 2026, 130, 1332−1345

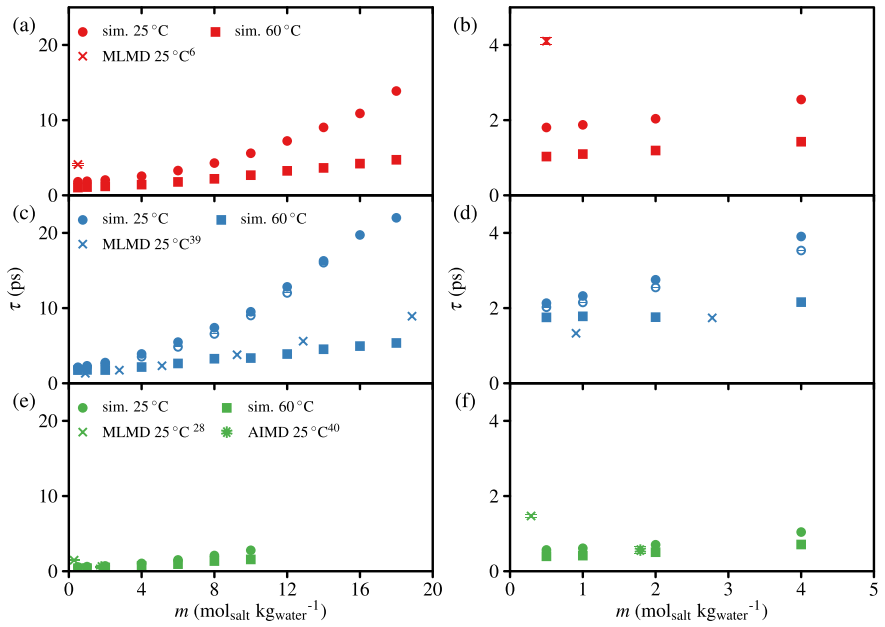

Figure 6. Hydroxide lifetimes in (a, b) KOH(aq) and (c, d) NaOH(aq) computed with a back-hopping bias $q = 0.4$ and (e, f) hydronium lifetimes in HCl(aq) determined with a back-hopping bias $q = 0.652$. (c, d) The results of the original NaOH(aq) force field at 25 °C are shown as well using open circles. The crosses and ten-point stars indicate results determined with MLMD[6,28,39] and AIMD,[40] respectively. Detailed differences at lower concentrations are shown on the right, providing better comparison of the AIMD and MLMD simulation results.

determined by the number of H atoms connected to the central O of the hydronium ion as well, as any of the 3 H atoms has to be involved in the reaction. Together, this yields $p_{H_3O^+} = (1 - q_{H_3O^+})/2 = 0.174$. The values for q and n are less obvious for OH^-, as there is a torus shaped area to which an incoming proton can be bound instead of n clearly distinct sites. However, OH^- is hydrogen bonded to the surrounding water molecules and the proton can only be donated by one of these surrounding waters through the hydrogen bonds. Instead of counting the number of possible locations where the hydrogen can be bound to the hydroxide, it is more practical to count the number of possible sources from which the hydrogen atom may originate. As Grotthuss transfer can only take place through these hydrogen bonds, we can assume that n_{OH^-} depends on the expected number of hydrogen bonds during Grotthuss transfer. Earlier works have shown that OH^- accepts 4 hydrogen bonds during Grotthuss transfer.[4,6,27] Therefore, in this work we take $n_{OH^-} = 4$, which results in $p_{OH^-} = (1 - q_{OH^-})/3$. The return probability of OH^- has been derived from earlier published MLMD trajectories[6] and is visualized in Figure 4d. From those trajectories, we determined that $q_{OH^-} = 0.4$, which results in $p_{OH^-} = 0.2$. The exact definition of what constitutes a complete Grotthuss transfer reaction event is somewhat arbitrary,[6,27,28,39] and would significantly alter q_{OH^-} and $q_{H_3O^+}$. Hence, comparing Grotthuss transferring ion lifetimes derived from inconsistent definitions does not provide meaningful insight. Here, we have used q and n proposed by Fischer et al.[40] Other studies[6,27,28,39] have used alternative approaches to identify irreversible, effective Grotthuss transfer events, which naturally lead to longer hydroxide and hydronium lifetimes as transient or ineffective transfer events are excluded.

The computed electrical conductivities are shown in Figure 5, together with experimental measurements[67,70] and fits through experimental data.[13,14] The OH^- and H_3O^+ lifetimes are calculated with eq 30, using the difference between experimentally measured electrical conductivities and electrical conductivities calculated from the classical molecular dynamics simulations. The results indicate that τ increases with concentration. This is expected, as the ratio between ion and water increases, it becomes less likely to create the required hydration modes for Grotthuss transfer to take place. This increase of τ for higher concentrations is also in agreement with literature.[27] Other ions are likely in the first or second hydration shell of the Grotthuss transferring ion, disrupting the hydrogen bonding and reducing the change for Grotthuss transfer. Such disruptions are found in ref 30, which showed that at high concentrations many hydrogen bonds are between hydroxide ions instead of between hydroxide and water. Protons cannot transfer from one OH^- to another OH^- as both ions already lack a proton. Similarly, the rearrangement of the hydrogen bonding network slows down with increasing concentrations, which results in increasing viscosity as well, and shown in (Figure 3). The definition for what constitutes a complete Grotthuss transfer greatly influences the Grotthuss transferring ion lifetime τ, which explains the significant variation in OH^- and H_3O^+ lifetimes indicated in Section 2. The computed H_3O^+ lifetime shows good agreement with the ab initio results in Fischer et al.[40] The H_3O^+ lifetime is 0.7 ps with our approach at 2 mol_{salt} kg_{water}^{-1}, where Fischer et al. determined a lifetime between 0.460 and 0.665 ps at a slightly lower concentration. However, Laage and co-workers[28] predicted significantly longer H_3O^+ lifetimes, 1.47 ps. This is logical as our approach and back-hopping probability matches that of Fischer et al.,[40] in contrast to the work by Laage and co-workers,[28] in which an integral over a time-correlation function was used in accordance with transition state theory which filters away less stable states. This results in a much stricter definition of Grotthuss transfer, yielding longer H_3O^+ lifetimes. Lagerweij et al.[6] used a strict definition of what constitutes a Grotthuss transfer as well. A double exponential decay fit on the time-correlation of transition between stable states was

https://doi.org/10.1021/acs.jpcb.5c07132
J. Phys. Chem. B 2026, 130, 1332−1345

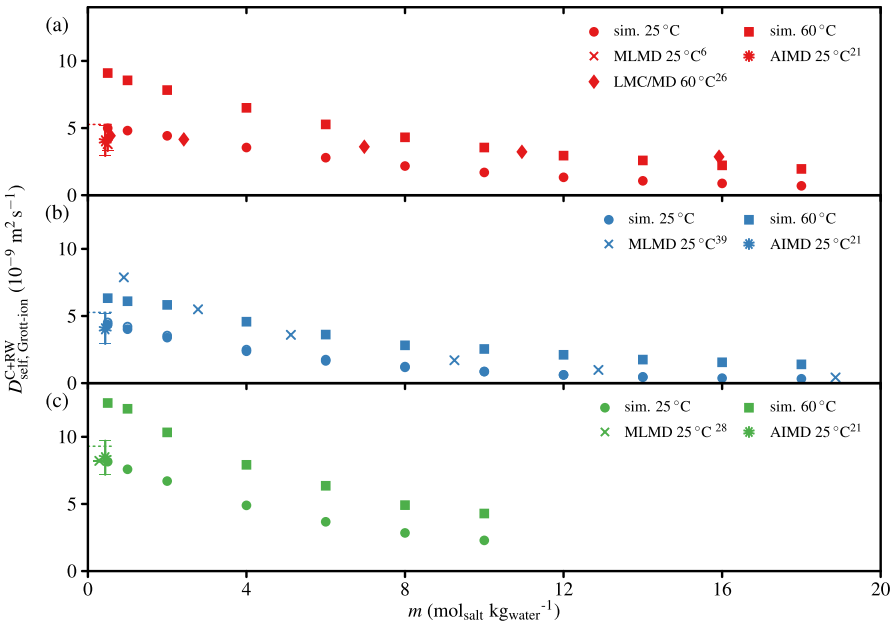

Figure 7. Self-diffusion coefficient of the Grotthuss transferring ions (a) KOH(aq), (b) NaOH(aq), and (c) HCl(aq). AIMD and MLMD simulation results taken from other works are shown as well.[6,21,28,39,40] (b) The results of the original NaOH(aq) force field at 25 °C are shown as well using open circles. The colored internal tick marks show experimental self-diffusion coefficients of these ions at infinite dilution[18] and 25 °C.

used, resulting in longer OH^- lifetimes than proposed by our method. The OH^- lifetime at 25 °C and 0.5 mol$_{salt}$ kg$_{water}^{-1}$ is 4.1 ps in ref 6, while here it is computed to be 1.8 ps for the same state point. The differences between the OH^- lifetimes presented in the present study and those NaOH(aq) reported by Hellström et al.[39] cannot be explained by comparing how the Grotthuss transfer events are analyzed. Reference 39 reports the use of a double exponential decay fit on a time-correlation of transition of stable states. Longer ion lifetimes would be expected with this approach, similar to refs 6, 28, however, the reported OH^- lifetimes are much shorter instead, 1.33 ps and not 2.3 ps as we found at 1 mol$_{salt}$ kg$_{water}^{-1}$. Figure 6c,d also shows that this difference is consistent for the entire simulated temperature range. Hellström et al.[39] reports results closer to our simulations at 65 °C compared to 25 °C. Hellström et al.[39] investigated the relevance of nuclear quantum effects (NQEs) for Grotthuss transfer, which resulted in even shorter OH^- lifetimes. Implementing NQEs increases the OH^- fraction with three hydrogen bonds, and this hydration mode is known to have low proton transfer energy barriers.[39] We compare to the results without NQEs, as the density functional used to train the MLIP has shown more accurate predictions of water properties without NQEs.[6,39,71] Further analysis of the simulations performed in ref 39 also reveals significant overestimation of the self-diffusion coefficient in the infinite dilution limit, and the follow-up work into electrical conductivities also showed significant overestimation compared to experimental measurements.[72] The differences in the OH^- lifetimes are therefore not caused by the definition of what constitutes Grotthuss transfer but by the implemented MLIP or the used density functional.

The computed self-diffusion coefficients of the Grotthuss transferring ions are shown in Figure 7. It clearly shows that our method correctly predicts self-diffusion coefficients at infinite dilution. While there are no accurate measurements of H_3O^+ and OH^- self-diffusion coefficients to compare to at other concentrations, the self-diffusion coefficients decrease with increasing concentration, which is the expected behavior for aqueous salt systems. Also, low concentration MLIP simulations between 0 and 1 mol$_{salt}$ kg$_{water}^{-1}$ at 25 °C of KOH(aq) and HCl(aq) are close to our results.[6,28] These low concentration MLIP simulations showed significantly higher OH^- and H_3O^+ lifetimes compared to our results. The method proposed in the present study resulted in very similar self-diffusion coefficients, while the ion lifetimes differ significantly, as shown in Figures 6 and 7. This indicates again how sensitive the ion lifetimes are for arbitrary choices in defining Grotthuss transfer, while self-diffusion coefficients provide a much more consistent comparison between how well MLIPs capture Grotthuss transfer. The only outlier in Figure 7 are the self-diffusion coefficients computed with the MLIP for NaOH(aq) by Hellström et al.[39] The self-diffusion coefficients of OH^- at 25 °C presented in ref 39. exceed our simulation results at 60 °C and our findings for H_3O^+ at 25 °C. The results in refs 39, 72. use the same MLIP and overestimate self-diffusion coefficients and electrical conductivities, while underestimating OH^- lifetimes. The simulation approach is comparable to refs 6, 28. while the results differ significantly. This indicates that differences in the results arise from the MLIP developed by Hellström et al.[39] These results were established using a MLIP, and it is unclear if these differences originates from the ab initio training data or the ML scheme implemented.

It is challenging to compare the diffusion coefficients computed here with the results presented by Dreßler and co-workers,[26] who used a Lattice Monte Carlo postprocessing approach to add structural transport to classical MD trajectories.[26] Reference 26 validated the Lattice Monte Carlo postprocessing by comparing self-diffusion coefficients of Grotthuss transferring computed with that method directly to AIMD simulation. To achieve this comparison, the temperature of the classical MD simulations was adjusted such that the self-diffusion coefficients of water matched those of the AIMD simulations in ref 26. The AIMD simulations in ref 26 were performed at 60 °C. However, the AIMD resulted

https://doi.org/10.1021/acs.jpcb.5c07132
J. Phys. Chem. B 2026, 130, 1332−1345

in significantly underestimated water self-diffusion coefficients. The classical MD simulations were therefore performed at much lower temperatures, ranging from −45 to 15 °C. These classical MD results with Lattice Monte Carlo postprocessing, also shown with red diamonds in Figure 7, clearly underestimate self-diffusion coefficients of OH^- in KOH(aq) if one compares to the results at 60 °C. It is noteworthy that the simulation at the lowest concentration actually simulated at 15 °C, and matches quite closely to the 25 °C result computed here. This may indicate that the approach in ref 26 is effectively as well, at low concentrations, if no such temperature shifts were performed.

It is already well established that $D_{self,Na^+} < D_{self,K^+}$[36] and this is also clearly shown in Figure 3. This logically results into differences in electrical conductivity between NaOH(aq) and KOH(aq). Our analysis also reveals that D_{self,OH^-} is also strongly impacted by concentration effects in NaOH(aq). The sodium seems to reduce the mobility of the water molecules, as also indicated by the increased viscosity. This in turn increases the time between effective Grotthuss transfer events.

5. CONCLUSIONS

This work shows how a combined approach of experimental measurements and classical molecular dynamics simulations can be used to investigate Grotthuss transfer effects. By implementing a relative simple postprocessing approach, we illustrated how classical force field-based molecular simulations can predict OH^- and H_3O^+ lifetimes and self-diffusion coefficients. This used to be limited to reactive force fields, machine-learned interatomic potentials or ab initio simulations. The present study proposes a method to use the well-understood limitation of classical force fields in modeling OH^- and H_3O^+ mixtures: only the vehicular transport of the ions is captured, while the ion transport due to Grotthuss transfer is neglected. We derived how a biased random walk can be used to describe the effects of the Grotthuss transfer on ion trajectories. The concentration and temperature dependence of the biased random walk is determined using the difference in electrical conductivity measured experimentally and computed using classical MD simulations. This difference is applied in eq 30 to compute the OH^- or H_3O^+ lifetimes and eq 31 to compute the ion self-diffusion coefficients. The computed self-diffusion coefficients match experimental results in the infinite dilution limit, and reveal differences in concentration effects between KOH(aq) and NaOH(aq). The well-known difference in electrical conductivity between KOH(aq) and NaOH(aq) does not only stem from the differences in diffusion of potassium and sodium ions, but also from the differences in the mobility of OH^-, which is much higher in KOH(aq) compared to NaOH(aq). This is caused by the effect of Na^+ on the hydrogen bonding network, resulting in high viscosities and low ion mobilities. This study also reports hydroxide and hydronium lifetimes. However, unlike self-diffusion coefficients, these depend on several microscopic properties of the Grotthuss transfer mechanism: the back-hopping probability, the number of reaction sites, and the average Grotthuss transfer distance. The ion lifetimes cannot be used to compare the quality of MLIPs and AIMD simulations because different definitions of what constitutes Grotthuss transfer are used in literature. Self-diffusion coefficients and electrical conductivities provide a more useful comparison because these macroscopic properties can be sampled accurately and the results are independent of different definitions of when Grotthuss transfer has occurred. Electrical conductivities can be directly compared to measurements, and thus provide the most reliable benchmark for a MLIP. However, computing electrical conductivities requires long simulation times. It may take more than 100 ns before the mean squared displacement of the Onsager coefficients has a slope of 1 in the log−log space. Earlier studies already indicated that more viscous systems, such as NaOH(aq) simulated here, require even longer simulation times.[16] Such long simulation times may currently be out of reach for MLMD simulations. Self-diffusion coefficients require less simulation time, and can be corrected for finite size effects. Therefore, self-diffusion coefficients are the most suitable property to compare how well MLIPs capture Grotthuss transfer. The method described in this study can be used to convert electrical conductivity measurements into self-diffusion coefficients to provide reference data.

■ ASSOCIATED CONTENT

Data Availability Statement

The data underlying this study are openly available in the 4TU Research Data database at https://doi.org/10.4121/e61b5dac-3a47-4ba7-ae98-9aaf782597ab.

Supporting Information

The Supporting Information is available free of charge at https://pubs.acs.org/doi/10.1021/acs.jpcb.5c07132.

Simulation settings of the classical MD simulations; and details on the force fields (PDF)

Simulation results per state point (XLSX)

■ AUTHOR INFORMATION

Corresponding Author

Thijs J.H. Vlugt − *Engineering Thermodynamics, Process & Energy Department, Faculty of Mechanical Engineering, Delft University of Technology, 2628CB Delft, The Netherlands;* orcid.org/0000-0003-3059-8712; Email: t.j.h.vlugt@tudelft.nl

Authors

V. Jelle Lagerweij − *Engineering Thermodynamics, Process & Energy Department, Faculty of Mechanical Engineering, Delft University of Technology, 2628CB Delft, The Netherlands;* orcid.org/0009-0000-6839-530X

Othonas A. Moultos − *Engineering Thermodynamics, Process & Energy Department, Faculty of Mechanical Engineering, Delft University of Technology, 2628CB Delft, The Netherlands;* orcid.org/0000-0001-7477-9684

Complete contact information is available at: https://pubs.acs.org/10.1021/acs.jpcb.5c07132

Notes

The authors declare no competing financial interest.

■ ACKNOWLEDGMENTS

This research was supported by The Netherlands Organization for Scientific Research (NWO) Domain Science, through access to national supercomputing facilities. We also gratefully acknowledge the computational resources provided by the DelftBlue supercomputer at the Delft High Performance Computing Center.

REFERENCES

(1) Greenwood, N. N.; Earnshaw, A. *Chemistry of the Elements*, 2nd ed.; Elsevier: Oxford UK, 2012.
(2) Marx, D. Proton Transfer 200 Years after von Grotthuss: Insights from Ab Initio Simulations. *ChemPhysChem* **2006**, *7*, 1848−1870.
(3) Tuckerman, M.; Laasonen, K.; Sprik, M.; Parrinello, M. Ab Initio Molecular Dynamics Simulation of the Solvation and Transport of H_3O^+ and OH^- Ions in Water. *J. Phys. Chem.* **1995**, *99*, 5749−5752.
(4) Tuckerman, M. E.; Chandra, A.; Marx, D. Structure and Dynamics of OH^-(Aq). *Acc. Chem. Res.* **2006**, *39*, 151−158.
(5) Marx, D.; Chandra, A.; Tuckerman, M. E. Aqueous Basic Solutions: Hydroxide Solvation, Structural Diffusion, and Comparison to the Hydrated Proton. *Chem. Rev.* **2010**, *110*, 2174−2216.
(6) Lagerweij, V. J.; Bougueroua, S.; Habibi, P.; Dey, P.; Gaigeot, M.-P.; Moultos, O. A.; Vlugt, T. J. H. From Grotthuss Transfer to Conductivity: Machine Learning Molecular Dynamics of Aqueous KOH. *J. Phys. Chem. B* **2025**, *129*, 6093−6099.
(7) Chatenet, M.; Pollet, B. G.; Dekel, D. R.; Dionigi, F.; Deseure, J.; Millet, P.; Braatz, R. D.; Bazant, M. Z.; Eikerling, M.; Staffell, I.; Balcombe, P.; Shao-Horn, Y.; Schäfer, H. Water Electrolysis: From Textbook Knowledge to the Latest Scientific Strategies and Industrial Developments. *Chem. Soc. Rev.* **2022**, *51*, 4583−4762.
(8) Schalenbach, M.; Zeradjanin, A. R.; Kasian, O.; Cherevko, S.; Mayrhofer, K. J. J. A Perspective on Low-Temperature Water Electrolysis − Challenges in Alkaline and Acidic Technology. *Int. J. Electrochem. Sci.* **2018**, *13*, 1173−1226.
(9) Almeida, M. F.; Xará, S. M.; Delgado, J.; Costa, C. A. Characterization of Spent AA Household Alkaline Batteries. *Waste Management* **2006**, *26*, 466−476.
(10) Kaneco, S.; Iiba, K.; Ohta, K.; Mizuno, T.; Saji, A. Electrochemical Reduction of CO_2 on Au in KOH + Methanol at Low Temperature. *J. Electroanal. Chem.* **1998**, *441*, 215−220.
(11) Passiniemi, P. Accurate Tracer Diffusion Coefficients of Na+ and Cl- Ions in Dilute Aqueous Sodium Chloride Solutions Measured with the Closed Capillary Method. *J. Solution Chem.* **1983**, *12*, 801−813.
(12) Haase, R.; Sauermann, P.-F.; Dücker, K.-H. Leitfähigkeiten Konzentrierter Elektrolytlösungen. *Zeitschrift f ü r Physikalische Chemie* **1965**, *47*, 224−245.
(13) DeWane, H. J.; Hamer, W. J. *Electrochemical Data, Part IV; Technical Report NIST*, 1966, Online available at: https://ntrs.nasa.gov/citations/19670002884.
(14) DeWane, J.; Hamer, W. J. *Electrochemical Data, Part 10; Technical Report NIST*, 1968, Online available at: https://ntrs.nasa.gov/citations/19690001083.
(15) Robinson, R. A.; Stokes, R. H. *Electrolyte Solutions the Measurement and Interpretation of Conductance, Chemical Potential, and Diffusion in Solutions of Simple Electrolytes.*, 2nd ed.; Butterworths: London UK, 1970.
(16) Blazquez, S.; Abascal, J. L. F.; Lagerweij, V. J.; Habibi, P.; Dey, P.; Vlugt, T. J. H.; Moultos, O. A.; Vega, C. Computation of Electrical Conductivities of Aqueous Electrolyte Solutions: Two Surfaces, One Property. *J. Chem. Theory Comput.* **2023**, *19*, 5380−5393.
(17) Gullbrekken, Ø.; Røe, I. T.; Selbach, S. M.; Schnell, S. K. Charge Transport in Water-NaCl Electrolytes with Molecular Dynamics Simulations. *J. Phys. Chem. B* **2023**, *127*, 2729−2738.
(18) Yuan-Hui, L.; Gregory, S. Diffusion of Ions in Sea Water and in Deep-Sea Sediments. *Geochim. Cosmochim. Acta* **1974**, *38*, 703−714.
(19) Chen, M.; Zheng, L.; Santra, B.; Ko, H.-Y.; DiStasio, R. A., Jr; Klein, M. L.; Car, R.; Wu, X. Hydroxide Diffuses Slower than Hydronium in Water Because Its Solvated Structure Inhibits Correlated Proton Transfer. *Nat. Chem.* **2018**, *10*, 413−419.
(20) Fischer, S. A.; Gunlycke, D. Analysis of Correlated Dynamics in the Grotthuss Mechanism of Proton Diffusion. *J. Phys. Chem. B* **2019**, *123*, 5536−5544.
(21) Muñoz-Santiburcio, D. Accurate Diffusion Coefficients of the Excess Proton and Hydroxide in Water via Extensive Ab Initio Simulations with Different Schemes. *J. Chem. Phys.* **2022**, *157*, No. 024504.
(22) Lazaridis, T.; Hummer, G. Classical Molecular Dynamics with Mobile Protons. *J. Chem. Inf. Model.* **2017**, *57*, 2833−2845.
(23) Dutta, A.; Lazaridis, T. Classical Models of Hydroxide for Proton Hopping Simulations. *J. Phys. Chem. B* **2024**, *128*, 12161−12170.
(24) Kabbe, G.; Dreßler, C.; Sebastiani, D. Toward Realistic Transfer Rates within the Coupled Molecular Dynamics/Lattice Monte Carlo Approach. *J. Phys. Chem. C* **2016**, *120*, 19905−19912.
(25) Kabbe, G.; Dreßler, C.; Sebastiani, D. Proton Mobility in Aqueous Systems: Combining Ab Initio Accuracy with Millisecond Timescales. *Phys. Chem. Chem. Phys.* **2017**, *19*, 28604−28609.
(26) Hänseroth, J.; Sebastiani, D.; Jimenez Siegert, J. A.; Scholl, J.; Skadell, K.; Dreßler, C. Hydroxide Mobility in Aqueous Systems: Combining Ab Initio Accuracy with Millisecond Timescales. *Small* **2025**, No. 2500931.
(27) Hellström, M.; Behler, J. Concentration-Dependent Proton Transfer Mechanisms in Aqueous NaOH Solutions: From Acceptor-Driven to Donor-Driven and Back. *J. Phys. Chem. Lett.* **2016**, *7*, 3302−3306.
(28) Gomez, A.; Thompson, W. H.; Laage, D. Neural-Network-Based Molecular Dynamics Simulations Reveal That Proton Transport in Water Is Doubly Gated by Sequential Hydrogen-Bond Exchange. *Nat. Chem.* **2024**, *16*, 1838−1844.
(29) Behler, J.; Parrinello, M. Generalized Neural-Network Representation of High-Dimensional Potential-Energy Surfaces. *Phys. Rev. Lett.* **2007**, *98*, No. 146401.
(30) Hänseroth, J.; Dreßler, C. Optimizing Machine Learning Interatomic Potentials for Hydroxide Transport: Surprising Efficiency of Single-Concentration Training. *J. Chem. Phys.* **2025**, *163*, No. 084118.
(31) Zeng, J.; Zhang, D.; Peng, A.; Zhang, X.; He, S.; Wang, Y.; Liu, X.; Bi, H.; Li, Y.; Cai, C.; Zhang, C.; Du, Y.; Zhu, J.-X.; Mo, P.; Huang, Z.; Zeng, Q.; Shi, S.; Qin, X.; Yu, Z.; Luo, C.; Ding, Y.; Liu, Y.-P.; Shi, R.; Wang, Z.; Bore, S. L.; Chang, J.; Deng, Z.; Ding, Z.; Han, S.; Jiang, W.; Ke, G.; Liu, Z.; Lu, D.; Muraoka, K.; Oliaei, H.; Singh, A. K.; Que, H.; Xu, W.; Xu, Z.; Zhuang, Y.-B.; Dai, J.; Giese, T. J.; Jia, W.; Xu, B.; York, D. M.; Zhang, L.; Wang, H. DeePMD-kit v3: A Multiple-Backend Framework for Machine Learning Potentials. *J. Chem. Theory Comput.* **2025**, *21*, 4375−4385.
(32) Anstine, D. M.; Isayev, O. Machine Learning Interatomic Potentials and Long-Range Physics. *J. Phys. Chem. A* **2023**, *127*, 2417−2431.
(33) Cheng, B. Latent Ewald Summation for Machine Learning of Long-Range Interactions. *npj Comput. Mater.* **2025**, *11*, 80.
(34) Zhang, C.; Tang, F.; Chen, M.; Xu, J.; Zhang, L.; Qiu, D. Y.; Perdew, J. P.; Klein, M. L.; Wu, X. Modeling Liquid Water by Climbing up Jacob's Ladder in Density Functional Theory Facilitated by Using Deep Neural Network Potentials. *J. Phys. Chem. B* **2021**, *125*, 11444−11456.
(35) Abascal, J. L. F.; Vega, C. A General Purpose Model for the Condensed Phases of Water: TIP4P/2005. *J. Chem. Phys.* **2005**, *123*, 234505.
(36) Habibi, P.; Rahbari, A.; Blazquez, S.; Vega, C.; Dey, P.; Vlugt, T. J. H.; Moultos, O. A. A New Force Field for OH^- for Computing Thermodynamic and Transport Properties of H_2 and O_2 in Aqueous NaOH and KOH Solutions. *J. Phys. Chem. B* **2022**, *126*, 9376−9387.
(37) Blazquez, S.; Conde, M. M.; Vega, C. Scaled Charges for Ions: An Improvement but Not the Final Word for Modeling Electrolytes in Water. *J. Chem. Phys.* **2023**, *158*, No. 054505.
(38) Blazquez, S.; de Lucas, M.; Vega, C.; Gámez, F. Acidifying the Madrid-2019 Force Field: A Rigid Model for H_3O^+ with Scaled Charges. *J. Chem. Phys.* **2025**, *162*, 171101.
(39) Hellström, M.; Ceriotti, M.; Behler, J. Nuclear Quantum Effects in Sodium Hydroxide Solutions from Neural Network Molecular Dynamics Simulations. *J. Phys. Chem. B* **2018**, *122*, 10158−10171.
(40) Fischer, S. A.; Dunlap, B. I.; Gunlycke, D. Correlated Dynamics in Aqueous Proton Diffusion. *Chemical Science* **2018**, *9*, 7126−7132.
(41) Halle, B.; Karlström, G. Prototropic Charge Migration in Water. Part 2.—Interpretation of Nuclear Magnetic Resonance and

https://doi.org/10.1021/acs.jpcb.5c07132
J. Phys. Chem. B 2026, 130, 1332−1345

Conductivity Data in Terms of Model Mechanisms. *Journal of the Chemical Society, Faraday Transactions 2: Molecular and Chemical Physics* **1983**, *79*, 1047−1073.
(42) Helfand, E. Transport Coefficients from Dissipation in a Canonical Ensemble. *Phys. Rev.* **1960**, *119*, 1−9.
(43) Chen, A.; Renshaw, E. The General Correlated Random Walk. *Journal of Applied Probability* **1994**, *31*, 869−884.
(44) Jamali, S. H.; Wolff, L.; Becker, T. M.; de Groen, M.; Ramdin, M.; Hartkamp, R.; Bardow, A.; Vlugt, T. J. H.; Moultos, O. A. OCTP: A Tool for On-the-Fly Calculation of Transport Properties of Fluids with the Order-n Algorithm in LAMMPS. *J. Chem. Inf. Model.* **2019**, *59*, 1290−1294.
(45) Frenkel, D.; Smit, B. *Understanding Molecular Simulation: From Algorithms to Applications*, 3rd ed.; Academic Press: San Diego, USA, 2023.
(46) Allen, M. P.; Tildesley, D. J. *Computer Simulation of Liquids*, 2nd ed.; Oxford University Press: New York, USA, 2017.
(47) Dünweg, B.; Kremer, K. Molecular Dynamics Simulation of a Polymer Chain in Solution. *J. Chem. Phys.* **1993**, *99*, 6983−6997.
(48) Yeh, I.-C.; Hummer, G. System-Size Dependence of Diffusion Coefficients and Viscosities from Molecular Dynamics Simulations with Periodic Boundary Conditions. *J. Phys. Chem. B* **2004**, *108*, 15873−15879.
(49) Celebi, A. T.; Jamali, S. H.; Bardow, A.; Vlugt, T. J. H.; Moultos, O. A. Finite-Size Effects of Diffusion Coefficients Computed from Molecular Dynamics: A Review of What We Have Learned so Far. *Mol. Simul.* **2021**, *47*, 831−845.
(50) Moultos, O. A.; Zhang, Y.; Tsimpanogiannis, I. N.; Economou, I. G.; Maginn, E. J. System-Size Corrections for Self-Diffusion Coefficients Calculated from Molecular Dynamics Simulations: The Case of CO_2, n-Alkanes, and Poly(Ethylene Glycol) Dimethyl Ethers. *J. Chem. Phys.* **2016**, *145*, No. 074109.
(51) Chakrapani, T. H.; Hajibeygi, H.; Moultos, O. A.; Vlugt, T. J. H. Impact of Finite-Size Effects on Computed Transport Properties: A Molecular Dynamics Study of Dilute Systems. *Mol. Phys.* **2025**, *123*, No. e2578408.
(52) Daivis, P. J.; Evans, D. J. Comparison of Constant Pressure and Constant Volume Nonequilibrium Simulations of Sheared Model Decane. *J. Chem. Phys.* **1994**, *100*, 541−547.
(53) Shao, Y.; Shigenobu, K.; Watanabe, M.; Zhang, C. Role of Viscosity in Deviations from the Nernst−Einstein Relation. *J. Phys. Chem. B* **2020**, *124*, 4774−4780.
(54) Krishna, R.; Wesselingh, J. A. The Maxwell-Stefan Approach to Mass Transfer. *Chem. Eng. Sci.* **1997**, *52*, 861−911.
(55) Krishna, R.; van Baten, J. M. The Darken Relation for Multicomponent Diffusion in Liquid Mixtures of Linear Alkanes: An Investigation Using Molecular Dynamics (MD) Simulations. *Ind. Eng. Chem. Res.* **2005**, *44*, 6939−6947.
(56) Plimpton, S. Fast Parallel Algorithms for Short-Range Molecular Dynamics. *J. Comput. Phys.* **1995**, *117*, 1−19.
(57) Thompson, A. P.; Aktulga, H. M.; Berger, R.; Bolintineanu, D. S.; Brown, W. M.; Crozier, P. S.; in 't Veld, P. J.; Kohlmeyer, A.; Moore, S. G.; Nguyen, T. D.; Shan, R.; Stevens, M. J.; Tranchida, J.; Trott, C.; Plimpton, S. J. LAMMPS - a Flexible Simulation Tool for Particle-Based Materials Modeling at the Atomic, Meso, and Continuum Scales. *Comput. Phys. Commun.* **2022**, *271*, No. 108171.
(58) Martínez, L.; Andrade, R.; Birgin, E. G.; Martínez, J. M. PACKMOL: A package for building initial configurations for molecular dynamics simulations. *J. Comput. Chem.* **2009**, *30*, 2157−2164.
(59) Padua, A.; Goloviznina, K.; Gong, Z. Fftool: XML Force Field Files v1.2.1. 2021; Online available at: .
(60) Ryckaert, J.-P.; Ciccotti, G.; Berendsen, H. J. C. Numerical Integration of the Cartesian Equations of Motion of a System with Constraints: Molecular Dynamics of n-Alkanes. *J. Comput. Phys.* **1977**, *23*, 327−341.
(61) Hockney, R. W.; Eastwood, J. W. *Computer Simulation Using Particles*, 1st ed.; CRC Press: Boca Raton, FL, 1988.
(62) Verlet, L. Computer "Experiments" on Classical Fluids. I. Thermodynamical Properties of Lennard-Jones Molecules. *Phys. Rev.* **1967**, *159*, 98−103.
(63) Nosé, S. A Unified Formulation of the Constant Temperature Molecular Dynamics Methods. *J. Chem. Phys.* **1984**, *81*, 511−519.
(64) Hoover, W. G. Canonical Dynamics: Equilibrium Phase-Space Distributions. *Phys. Rev. A* **1985**, *31*, 1695−1697.
(65) de Lucas, M.; Blazquez, S.; Troncoso, J.; Vega, C.; Gámez, F. Dressing a Nonpolarizable Force Field for OH^- in TIP4P/2005 Aqueous Solutions with Corrected Hirshfeld Charges. *J. Phys. Chem. Lett.* **2024**, *15*, 9411−9418.
(66) Laliberté, M. Model for Calculating the Viscosity of Aqueous Solutions. *Journal of Chemical & Engineering Data* **2007**, *52*, 321−335.
(67) Zaytsev, I. D.; Aseyev, G. G. *Properties of Aqueous Solutions of Electrolytes*, 1st ed.; CRC Press, 1992.
(68) Dreßler, C.; Sebastiani, D. Effect of Anion Reorientation on Proton Mobility in the Solid Acids Family $CsH_y XO_4$ (X = S, P, Se, y = 1, 2) from Ab Initio Molecular Dynamics Simulations. *Phys. Chem. Chem. Phys.* **2020**, *22*, 10738−10752.
(69) Kumar, R.; Schmidt, J. R.; Skinner, J. L. Hydrogen Bonding Definitions and Dynamics in Liquid Water. *J. Chem. Phys.* **2007**, *126*, 204107.
(70) Dobos, D. *Electrochemical Data: A Handbook for Electrochemists in Industry and Universities*; Elsevier Scientific Pub. Co.: Amsterdam, 1975.
(71) Marsalek, O.; Markland, T. E. Quantum Dynamics and Spectroscopy of Ab Initio Liquid Water: The Interplay of Nuclear and Electronic Quantum Effects. *J. Phys. Chem. Lett.* **2017**, *8*, 1545−1551.
(72) Shao, Y.; Hellström, M.; Yllö, A.; Mindemark, J.; Hermansson, K.; Behler, J.; Zhang, C. Temperature Effects on the Ionic Conductivity in Concentrated Alkaline Electrolyte Solutions. *Phys. Chem. Chem. Phys.* **2020**, *22*, 10426−10430.